CHEMICAL ENGINEERING TRANSACTIONS
VOL. 117, 2025
A publication of AIDIC
The Italian Association of Chemical Engineering
Online at www.cetjournal.it
Guest Editors: Fabrizio Bezzo, Flavio Manenti, Gabriele Pannocchia, Almerinda di Benedetto

ISBN 979-12-81206-17-5; **ISSN** 2283-9216
DOI: 10.3303/CET25117147

Hydrothermal Synthesis of High-Performance 3D Black TiO_2/rGO Solar Absorber for Solar-Driven Interfacial Water Evaporation

Wesley J. Lawrence, Fisseha A. Bezza, Shepherd M. Tichapondwa, Evans M. N. Chirwa*

Water Utilisation and Environmental Engineering Division, Department of Chemical Engineering, University of Pretoria, Pretoria 0002, South Africa
evans.chirwa@up.ac.za

Fresh water around the globe has become a resource which is in short supply, and this is being further aggravated by rapid economic and population growth, industrialisation, and urbanisation. Desalination has long been realised as a solution to the fresh water crisis and implementation has swiftly increased. Traditional solar-driven desalination technologies are extremely inclined to low efficiencies due to the dissipation of solar energy into the non-evaporative bulk water. Solar-driven interfacial water evaporation hinges on the principle of heat localisation at the water-air interface which in turn leads to extraordinary photothermal conversion potential and water evaporation rates. This study aims to demonstrate the potential of high-performance solar energy utilisation through the development of a highly efficient solar absorber. By hydrothermally reducing a graphene oxide (GO) suspension containing black titanium dioxide (black TiO_2) particles, a 3D hybrid solar absorber can be fabricated. The 3D hybrid composite was characterised using various techniques to evaluate its structure and morphology, surface area, and solar absorption potential. The solar-driven interfacial water evaporation system demonstrated a high photothermal conversion efficiency of 82.38 % when exposed to 1-sun illumination and an evaporation rate of 1.19 kg/m^2·h. The encouraging performance displayed by the 3D solar absorber is owed to the high optical absorption of the whole UV and visible wavelength region.

1. Introduction

Fresh water is in short supply around the world. The availability of fresh water is continuously diminishing due to rapid population growth with its associated rise in demand, industrialisation, and urbanisation. The traditional solar-driven water evaporation systems produce steam by means of bottom heating or volumetric heating of the bulk water body (He et al., 2021). These systems are highly susceptible to low-efficiency rates due to the wastage of solar energy when the non-evaporative bulk water is heated. To overcome this, interfacial solar-driven desalination centres around the localisation of heat at the water-air interface which in turn leads to extraordinary photothermal conversion potential and evaporation rates by minimising the conductive heat loss to the bulk water. A solar-driven interfacial evaporation system comprises a solar absorber/evaporator with efficient solar absorption potential, and an adequate thermal insulation system, circumventing heat loss to the bulk water body while localising the solar-to-thermal conversion process at the liquid water interface. Additionally, to further improve performance and minimise heat loss a floating support is required with the ability to simultaneously maximise the evaporation rate and transfer of liquid to the evaporative surface (Yin et al., 2021).
Photothermal materials are the most essential elements in the solar-driven interfacial desalination process and ideally should exhibit good solar absorbance across the UV and visible light spectrum and low thermal emittance. Another crucial attribute is the rapid water-molecule transportation and extremely porous structure of the material which facilitates water transfer to the evaporative surface and increases the evaporation rate. Recently, black titanium dioxide (black TiO_2) has obtained great interest due to its wide-spectrum activity, low

Paper Received: 3 December 2024; Revised: 11 February 2025; Accepted: 3 May 2025
Please cite this article as: Lawrence W.J., Bezza F.A., Tichapondwa S.M., Chirwa E.M.N., 2025, Hydrothermal Synthesis of High-Performance 3D Black TiO2/rGO Solar Absorber for Solar-Driven Interfacial Water Evaporation , Chemical Engineering Transactions, 117, 877-882 DOI:10.3303/CET25117147

cost and toxicity, and stability making it ideal for use as a photothermal material. Black TiO_2 addresses the wide band-gap problem of white TiO_2 (Tabana and Tichapondwa, 2023) through the introduction of Ti^{3+} defects and oxygen vacancies into the titanium oxide lattice (Shen et al., 2017). Carbon-based materials are extremely popular photothermal materials as they exhibit broadband absorbance capacity and exceptional chemical stability. Graphene is a single-atom-thick 2D carbon material boasting high electrical and thermal conductivity and a large specific surface area which makes it an ideal photothermal material for use in solar-driven interfacial desalination. The formation of 3D graphene nanosheets and 3D graphene-based structures presents excellent photothermal performance and interfacial desalination ability owing to the increased mass and heat transfer channels along with a greater light scattering distance. The hybridisation of reduced graphene oxide (rGO) with black TiO_2 has presented enhanced photothermal conversion performance and solar steam generation (Liu et al., 2018).

2. Materials and Methods

2.1 Materials

Potassium permanganate ($KMnO_4$ ≥ 99 %), sulphuric acid (H_2SO_4 > 98 %), ortho-phosphoric acid (H_3PO_4 ≥ 85 %), sodium chloride (NaCl ≥ 99 %), hydrochloric acid (HCl, 30 w.%), and hydrogen peroxide (H_2O_2, 30 w.%) were sourced from Glassworld, South Africa. Titanium (IV) oxide powder (Anatase ≥ 99 %), graphite powder, and sodium borohydride ($NaBH_4$ > 98 %) were supplied by Sigma Aldrich. Deionised water was used for all experiments.

2.2 Synthesis of GO

Graphene oxide was synthesised using Tours' method adapted from Habte et al. (2019). In short, a mixture of 360 mL of concentrated H_2SO_4 and 40 mL of concentrated H_3PO_4 was prepared by magnetically stirring. This was followed by adding 3 g graphite powder and 18 g $KMnO_4$ into the mixture, resulting in a temperature increase between the range of 40 – 45 °C. Subsequently, the mixture was placed in a temperature-controlled incubator shaker and heated to 50 °C while being continuously stirred for 24 h. Afterwards, 400 mL of ice water was added to the mixture followed by 30 mL of 30 W.% H_2O_2. The resulting product was centrifuged and the supernatant decanted, the solid left was washed with HCl and once with water.

2.3 Synthesis of black TiO_2

Black TiO_2 was synthesised using $NaBH_4$ reduction of commercial grade TiO_2, which was adapted from the method described (Shen et al., 2017). Briefly, 5 g of white TiO_2 was rigorously mixed with 4 g of $NaBH_4$, this was then poured into a porcelain boat and placed in a chamber oven at 400 °C for 4 h in a N_2 environment. The final product was cooled, washed with water, dried, and powdered.

2.4 Fabrication of 3D black TiO_2/rGO

The synthesis using hydrothermal reduction involved dissolving 10 g of GO in water using ultrasound dispersion for 1 h at room temperature. Thereafter, 10 g of black TiO_2 powder was added to the solution and sonicated for 1 h which guaranteed even dispersion of the black TiO_2 particles within the solution. The GO suspension was then transferred to a 300 mL Teflon-lined autoclave, sealed, and incubated at 170 °C for 19 h. The final product was freeze-dried for 72 h.

2.5 Characterisation

The materials were characterised to determine their morphology, phase, BET surface area, and solar absorption performance. Scanning electron microscopy Zeiss Ultra Plus FEG SEM and transmission electron microscopy JOEL JEM 2100F TEM were used to study the morphology and structure of the as-synthesised samples. Powder X-ray diffraction (XRD) spectra were determined using a Bruker D2 Phaser with Cu-Kα radiation (λ = 0.154184 nm). Data was collected in the angular range of 10 to 80° 2θ with a step size of 0.05° 2θ and the phase identification was carried out using the X-ray diffraction software package Match!4 (Crystal Impact, Bonn, Germany). The specific surface area of the sample was determined using the dynamic Brunauer-Emmett-Teller (BET) method with an N_2 adsorption isotherm at 150 °C collected with a NOVA Touch LX2 system. The solar absorption performance of the samples was assessed over a wavelength range of 250 – 800 nm using Ultraviolet-visible diffuse reflectance spectroscopy (UV-Vis DRS) on a U-3900 Spectrophotometer (Hitachi, Japan).

2.6 Solar-driven interfacial evaporation test

The solar-driven interfacial evaporation performance of the 3D hybrid solar absorber was investigated using a xenon-arc lamp-based solar simulator under 1-sun illumination. The interfacial desalination test was carried out

for a total time duration of 12 h in four rounds, each consisting of 3 h. The 3D black TiO_2/rGO cylindrical absorber (6.8 × 3.0 cm) was positioned horizontally on a cellulose floating support exhibiting low thermal conductivity (0.043 W/m·K) and high hydrophilicity which was then placed in a beaker with saline water. To simulate highly saline seawater for the desalination study, water was thoroughly mixed with 35 wt.% NaCl. The cellulose support prevents direct contact between the bulk water and the solar absorber, preventing heat dissipation while guaranteeing continuous water supply to the solar absorber. The beaker was then enclosed in a transparent glass cover to reduce convective heat loss. The glass cover was sealed using vacuum seal grease to further minimise convective heat loss to the environment. The mass of vapour generated was weighed after condensation using a digital balance and the surface temperature of the solar absorber was recorded using an infrared thermal imaging camera every 30 min.

3. Results and Discussion

3.1 Phase, structure and morphology analyses

Figure 1a shows the SEM image of the black TiO_2/rGO composite and displays a fluffy and wrinkled morphology, illustrating the large surface area which is favourable for increased water and heat absorption potential. The observed large surface area was further confirmed by the BET surface area of 22.1 m^2/g and a pore volume of 0.054 cm^3/g was attained. The specific surface area and porosity of the composite are highly favourable for effective capillary force-driven water transportation and efficient solar-to-thermal conversion as water channels through and fills the connected pores of the solar absorber (Yan et al., 2023). Further observation of the SEM image reveals black TiO_2 particles are uniformly anchored to the outer and inner walls of the rGO sheets owing to a strong interaction between the hydrophilic functional groups on GO and the hydroxyl groups on black TiO_2 (Zhang et al., 2021).

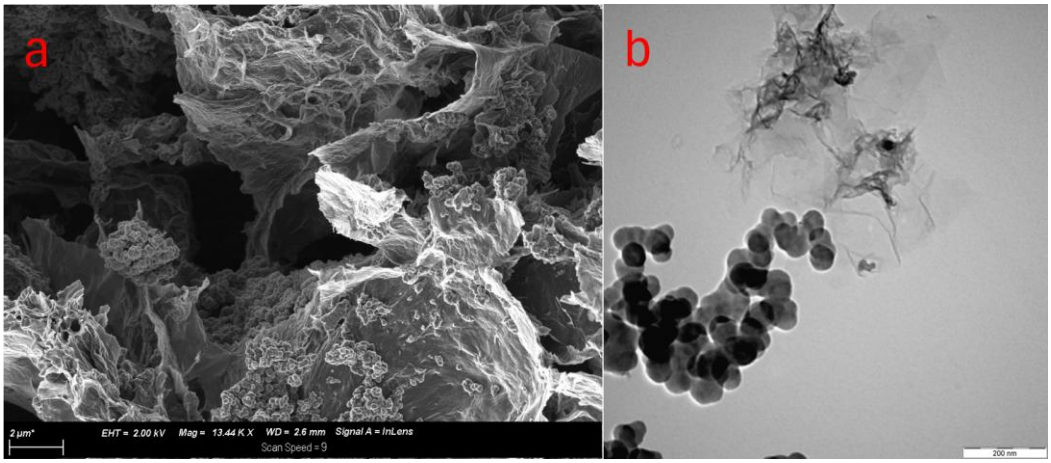

Figure 1: SEM (a) and TEM (b) analysis of black TiO_2/rGO.

The TEM image of the 3D hybrid composite (Figure 1b) revealed a heterogeneous structure with large agglomerates of black TiO_2 particles distributed on the surface of the rGO nanosheets. The black TiO_2 particles observed ranged in size between 10 and 60 nm with distinct structures to that of anatase TiO_2.

The crystallinity and phase composition of the composite material were analysed using XRD (Figure 2). The sharp peaks demonstrated the high crystallinity of the sample. The X-ray diffractograms of the hybrid composite revealed the presence of the anatase TiO_2 phase only. The sharp diffraction peak located at $2\theta = 27°$ was assigned to the (002) crystal plane of graphitic carbon due to the presence of rGO in the composite (Hidayat et al., 2022). The black TiO_2/rGO composite peaks correspond to anatase, GO and rGO peaks indicating a lack of impurities introduced during the synthesis process.

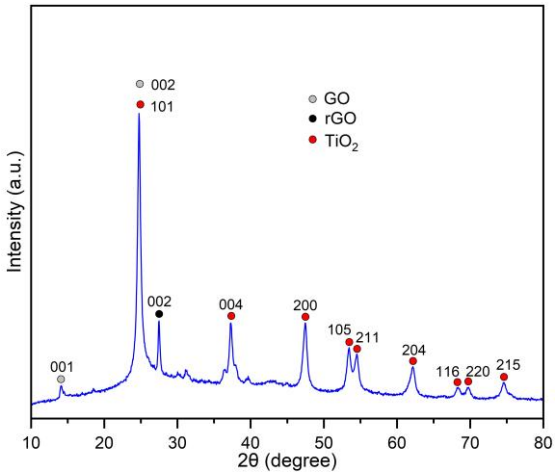

Figure 2: X-ray diffraction pattern of black TiO_2/rGO.

3.2 Solar absorption potential

Figure 3a shows the solar absorption performance of the hybrid composite. The composite displayed a considerable increase in light absorption across the UV and visible wavelength range compared to white TiO_2 and rGO. The composite showed exceptional solar absorption over the whole range of UV-Vis DRS regions which is essential for efficient solar-driven interfacial water evaporation (Cong et al., 2007).

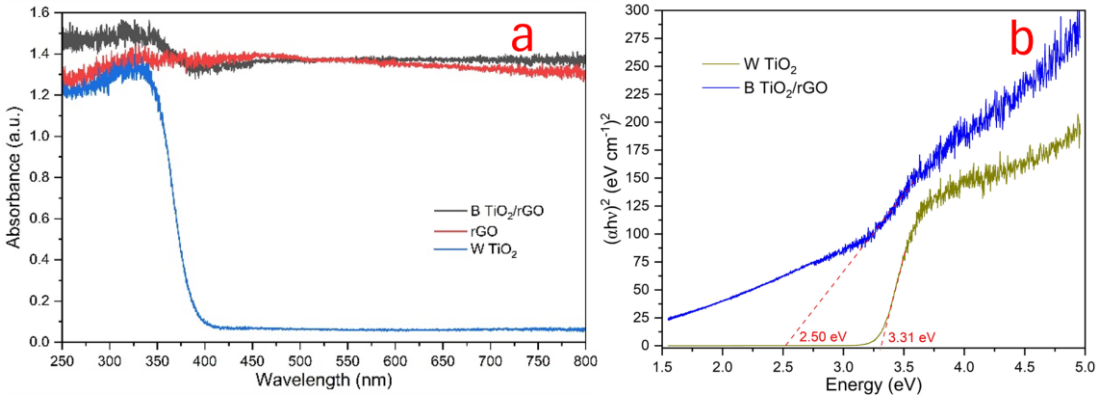

Figure 3: UV-Vis DRS spectra of rGO, white TiO_2, and black TiO_2/rGO (a) and band-gap energy of white TiO_2 and black TiO_2/rGO estimated from their corresponding Tauc plots (b).

A semiconductor's band-gap energy indicates the energy necessary to excite an electron from the valence band to the conduction band. Using the relationship shown in Eq(1), a Tauc plot can be produced to determine the band gap value of the composite (Makuła et al., 2018).

$$(\alpha h\nu)^{1/\gamma} = \beta(h\nu - E_g) \quad (1)$$

Where α is the absorption coefficient, h is Planck's constant (6.626×10^{-34} J·s), ν is the photon's frequency, β is a constant, E_g is the band-gap energy (eV). The factor γ is determined by the nature of the electron transition and is allocated values of 0.5 or 2 for direct and indirect band gaps, respectively. The direct band gaps for white TiO_2 and black TiO_2/rGO were determined using the Tauc plots generated from their UV-Vis DRS spectra. As shown in Figure 3b, the black TiO_2/rGO composite had a band gap of ~2.50 eV which is considerably lower than that of the pristine anatase TiO_2 band-gap value (3.31 eV). The reduced band gap energy indicates easier photoexcitation of charge carriers with low energy.

3.3 Solar-driven interfacial evaporation potential

The most important parameters for evaluating the interfacial water evaporation performance are the solar-driven water evaporation rate and the photothermal conversion efficiency. The water evaporation rate is the mass flux

due to the evaporation of water. The photothermal conversion efficiency can be determined by analysing the ratio of the stored thermal energy in the generated vapour to the incoming solar flux, which can be calculated based on the following relationship (Farabi et al., 2024).

$$\dot{m} = \frac{\Delta m}{s \times t} \tag{2}$$

Where Δm is the change of mass due to water evaporation (kg), s is the effective absorption area (m^2), and t is the solar irradiation time (h).

$$\eta = \frac{\dot{m} h_{Lv}}{q_i} \times 100\ \% \tag{3}$$

Where η is the photothermal conversion efficiency, $\dot{m}$ refers to the evaporation rate of water ($kg/m^2 \cdot h$), h_{Lv} refers to the total liquid-vapour phase-change enthalpy, q_i is incident solar power density, with the value of 1 kW/m^2.

$$h_{Lv} = C\Delta T + h_{vap} \tag{4}$$

Where C is the specific heat capacity of water (4.2 J/g·K), ΔT is the temperature rise of water and h_{vap} is the vaporisation enthalpy at the surface of the porous macrostructure. The water vapour generated (as displayed in Figure 4b) was determined to be 1.19 $kg/m^2 \cdot h$, the total liquid-vapour phase-change enthalpy (h_{Lv}) was determined to be 2496 (kJ/kg), and the photothermal conversion efficiency is 82.38 %.

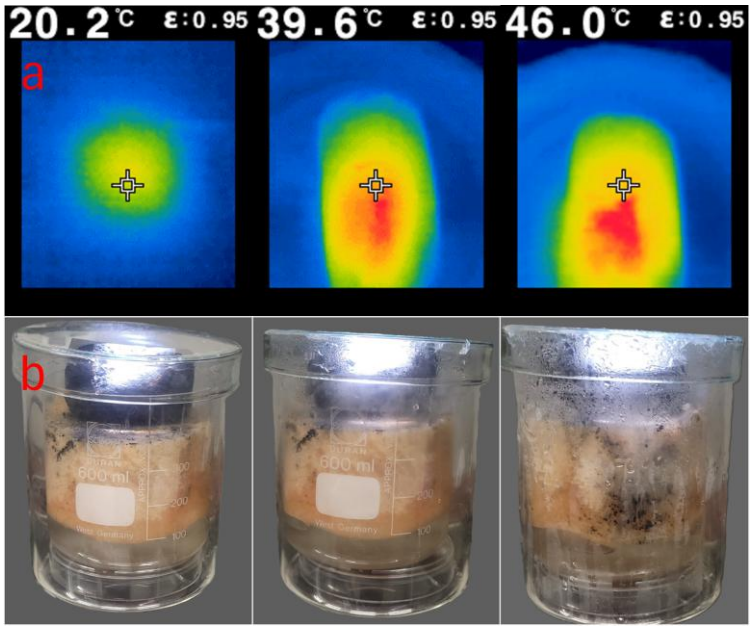

Figure 4: Infrared thermal images of the surface temperature of the 3D black TiO_2/rGO absorber taken every 30 min (a) and the corresponding digital images of the solar-driven interfacial desalination test (b).

The obtained photothermal conversion efficiency of 82.38 % is significantly greater than the performance observed in other studies (Zhu et al., 2016). High solar-to-thermal conversion efficiency is obtained by maximising the total solar absorbance and at the same time, minimising the thermal radiation and conduction loss. The 3D solar absorber showed a high surface temperature increase from 20.2 to 46 °C within 90 min, as displayed in Figure 4a, and remained constant over the 180-min interfacial-desalination test. The rapid surface temperature increase at the surface of the evaporator is the driving force for the continuous flow of water from the bulk water body via the cellulose channel. This is the result of the efficient solar absorption potential of the 3D solar absorber, demonstrating its remarkable photothermal performance. The high photothermal conversion efficiency and steam generation potential of the solar evaporator can be attributed to the highly porous structure and the synergistic photocatalytic activity of the black TiO_2 and rGO composite. The efficient water transfer as well as the thermal insulation provided by the cellulose support plays a significant role in avoiding heat loss to the bulk water and localizing the heat generated on the water-air surface. The reduction of TiO_2 into black TiO_2 bestows it with superb broadband solar absorption potential which makes it ideal for photothermal application.

4. Conclusions

The 3D composite solar absorber synthesised in this study illustrates its promising potential for solar-driven interfacial desalination as it displayed a high photothermal conversion efficiency of 82.38 % under 1-sun illumination and an evaporation rate of 1.19 kg/m^2·h. The astonishingly high photothermal conversion efficiency is a result of the porous morphology of the 3D macrostructure which induces multidirectional light absorption and numerous reflections of incident light which ensures that the energy lost is significantly decreased. The performance shown by the 3D solar absorber is accredited to the high-water transferability, and thermal localisation on the surface of the evaporator due to insulation. The effective thermal management provided by thermal insulation was ensured by the cellulose sponge support, which minimised the radiative and convective heat loss to the environment while preventing the dissipation of heat into the bulk water. The 3D porous macrostructure shows promising avenues for large-scale application of water desalination, making it possible to utilise abundant solar energy to produce fresh water from saline water sources and overcome the water shortage challenge.

References

Cong, Y., Zhang, J., Chen, F., Anpo, M., & He, D. (2007). Preparation, photocatalytic activity, and mechanism of nano-TiO2 Co-doped with nitrogen and iron (III). *Journal of Physical Chemistry C*, *111*(28), 10618–10623.

Farabi, S. N., Habib, K., Mim, M., Zaed, M. A., Ali, S. A., Younas, M., & Saidur, R. (2024). The future of solar-driven interfacial steam generation for sustainable water desalination: Drivers, challenges, and opportunities-review. In *Results in Engineering* (Vol. 23). Elsevier B.V.

Habte, A. T., Ayele, D. W., & Hu, M. (2019). Synthesis and Characterization of Reduced Graphene Oxide (rGO) Started from Graphene Oxide (GO) Using the Tour Method with Different Parameters. *Advances in Materials Science and Engineering*, *2019*.

He, C., Liu, Z., Wu, J., Pan, X., Fang, Z., Li, J., & Bryan, B. A. (2021). Future global urban water scarcity and potential solutions. *Nature Communications*, *12*(1).

Hidayat, R., Wahyuningsih, S., Fadillah, G., & Ramelan, A. H. (2022). Highly Visible Light Photodegradation of RhB as Synthetic Organic Dye Pollutant Over TiO2-Modified Reduced Graphene Oxide. *Journal of Inorganic and Organometallic Polymers and Materials*, *32*(1), 85–93.

Liu, X., Hou, B., Wang, G., Cui, Z., Zhu, X., & Wang, X. (2018). Black titania/graphene oxide nanocomposite films with excellent photothermal property for solar steam generation. *Journal of Materials Research*, *33*(6), 674–684.

Makuła, P., Pacia, M., & Macyk, W. (2018). How To Correctly Determine the Band Gap Energy of Modified Semiconductor Photocatalysts Based on UV-Vis Spectra. In *Journal of Physical Chemistry Letters* (Vol. 9, Issue 23, pp. 6814–6817).

Shen, L., Xing, Z., Zou, J., Li, Z., Wu, X., Zhang, Y., Zhu, Q., Yang, S., & Zhou, W. (2017). Black TiO2 nanobelts/g-C3N4 nanosheets Laminated Heterojunctions with Efficient Visible-Light-Driven Photocatalytic Performance. *Scientific Reports*, *7*(41978).

Tabana L.S., Tichapondwa S.M., 2023, Photocatalytic Degradation of Phenol using Visible light Activated Ag-AgBr-Hydrotalcite Composite, Chemical Engineering Transactions, 99, 259-264.

Yan, J., Wu, Q., Wang, J., Xiao, W., Zhang, G., Xue, H., & Gao, J. (2023). Carbon nanofiber reinforced carbon aerogels for steam generation: Synergy of solar driven interface evaporation and side wall induced natural evaporation. *Journal of Colloid and Interface Science*, *641*, 1033–1042.

Yin, H., Xie, H., Liu, J., Zou, X., & Liu, J. (2021). Graphene tube shaped photothermal layer for efficient solar-driven interfacial evaporation. *Desalination*, *511*(115116).

Zhang, D., Zhang, M., Chen, S., Liang, Q., Sheng, N., Han, Z., Cai, Y., & Wang, H. (2021). Scalable, self-cleaning and self-floating bi-layered bacterial cellulose biofoam for efficient solar evaporator with photocatalytic purification. *Desalination*, *500*(114899).

Zhu, G., Xu, J., Zhao, W., & Huang, F. (2016). Constructing black titania with unique nanocage structure for solar desalination. *ACS Applied Materials and Interfaces*, *8*(46), 31716–31721.